Article

Rape (*Brassica napus* L.) Growth Monitoring and Mapping Based on Radarsat-2 Time-Series Data

Wangfei Zhang [1,2] , Erxue Chen [2], Zengyuan Li [2,*], Lei Zhao [2], Yongjie Ji [1], Yahong Zhang [1] and Zhiqin Liu [3]

1   College of Forestry, Southwest Forestry University, Kunming 650224, China; mewhff@163.com (W.Z.);
    jiyongjie@live.cn (Y.J.); yuezhizhuh@163.com (Y.Z.)
2   Institute of Forest Resource Information Techniques, Chinese Academy of Forestry, Beijing 100091, China;
    chenerx@caf.ac.cn (E.C.); zhaoleiiam@126.com (L.Z.)
3   College of Ecology and Soil &Water Conservation, Southwest Forestry University, Kunming 650224, China;
    lzq-xl@163.com
*   Correspondence: zengyuan.li@caf.ac.cn; Tel./Fax: +86-10-6288-9163

Abstract: In this study, 27 polarimetric parameters were extracted from Radarsat-2 polarimetric synthetic aperture radar (SAR) at each growth stage of the rape crop. The sensitivity to growth parameters such as stem height, leaf area index (LAI), and biomass were investigated as a function of days after sowing. Based on the sensitivity analysis, five empirical regression models were compared to determine the best model for stem height, LAI, and biomass inversion. Of these five models, quadratic models had higher R^2 values than other models in most cases of growth parameter inversions, but when these results were related to physical scattering mechanisms, the inversion results produced overestimation in the performance of some parameters. By contrast, linear and logarithmic models, which had lower R^2 values than the quadratic models, had stable performance for growth parameter inversions, particularly in terms of their performance at each growth stage. The best biomass inversion performance was acquired by the volume component of a quadratic model, with an R^2 value of 0.854 and root mean square error (RMSE) of 109.93 g m^{-2}. The best LAI inversion was also acquired by a quadratic model, but used the radar vegetation index (Cloude), with an R^2 value of 0.8706 and RMSE of 0.56 m^2 m^{-2}. Stem height was acquired by scattering angle alpha (α) using a logarithmic model, with an R^2 of 0.926 value and RMSE of 11.09 cm. The performances of these models were also analysed for biomass estimation at the second growth stage (P2), third growth stage (P3), and fourth growth stage (P4). The results showed that the models built at the P3 stage had better substitutability with the models built during all of the growth stages. From the mapping results, we conclude that a model built at the P3 stage can be used for rape biomass inversion, with 90% of estimation errors being less than 100 g m^{-2}.

Keywords: rape (*Brassica napus* L.); monitoring; biomass; stem height; LAI; empirical regression model; inversion

---

1. Introduction

Rape (*Brassica napus* L.) has been the second largest source of protein and the third leading source of vegetable oil in the world since 2000, according to the United States Department of Agriculture [1]. Its planting area has increased in recent years; therefore, the importance of this crop to global markets is clearly increasing, and as such, there has been much interest in accurately monitoring its growth and estimating yields. Crop yield is a critical indicator of national food security and food trade [2]. Forecasting yield is not a trivial task, especially given that the global population is expected to reach about 9 billion in 2050 [3,4]. As good indicators of crop potential yield, crop

biomass, leaf area index (LAI), and stem height have been analysed in many studies [5,6]. However, the direct measurement of these growth parameters is destructive and expensive, which has resulted in significant interest in obtaining this kind of information by Earth observation data using remote sensing techniques [7–10]. Wang et al. (2016) retrieved maize biomass with hyperspectral and lidar data, and the estimated root mean square error (RMSE) was 321.092 g m^{-2} [7]. Xia et al. (2017) estimated wheat LAI, and the estimated RMSE was less than 24% [8]. Cable et al. (2014) interpreted the sensitivity of synthetic aperture radar (SAR) backscatter coefficients and decomposition parameters to crop growth parameters [9,10]. Among the available Earth observation data, SAR data, with its attributes of all-weather monitoring and vegetation structure sensitivity, have attracted the most interest in the monitoring of crop condition, production, and yield forecasting in recent years [3,6,7,11,12]. The correlations among biomass, LAI, and backscatter from the K-, Ku-, X-, C-, and L- frequencies were analysed and reported when SAR was first applied. The crops involved included wheat, rice, corn, and soybean. Strong correlations were found between microwave backscatter and both corn and biophysical parameters such as LAI and biomass. Thus, microwave backscattter was useful for retrieving different growth parameters; however, it has proven difficult to interpret the physical reason for the inversion results, which has limited their development for crop growth parameter inversion, particularly when there is more than one scattering mechanism operating [13–17]. With development of the quad-polarisation technique, several quad-polarimetric based parameters such as the radar vegetation index (RVI), pedestal height, volume scattering components, and scattering entropy have been extracted to investigate their sensitivity to crop growth parameters because of their sensitivity to vegetation scattering mechanisms in the C-Band [1,18,19]. The vegetation scattering mechanisms are related to vegetation structures. The strong interpretative ability of quad-polarimetric parameters for the multiple scattering mechanisms within a vegetation covered surface has suggested its potential for crop monitoring [2,14,15,20–24]. Jiao et al. (2011) reported the good performance of 18 quad-polarisation parameters in corn and soybean LAI estimation using linear regression models [8]. Wiseman et al. (2014) observed the correlations between 21 quad-polarimetric parameters and the biomass of canola (Canadian rape), corn, soybean, and wheat [2]. Canisius et al. (2017) reported the good performance for scattering angle alpha (α) in wheat and canola stem height inversion [18]. These studies also revealed the variability of scattering mechanisms due to the vegetation structure varying by crop type, condition, and phenology [2,11].

Rape (*Brassica napus* L.) is very different from rice, wheat, and soybean, as it is a broadleaf plant with an obvious distinctive change in canopy structure during the growing season. Its LAI reaches a maximum at the beginning of flowering, and declines with the loss of lower leaves when seed development begins. Because of its individuality and obvious variability at different growth stages, it is necessary to analyse its polarimetric response during the whole growth cycle and also at key growth stages to obtain an accurate estimation of its growth parameters [2,25]. Canisius et al. (2017) compared the performance of polarimetric parameters for LAI and stem height inversion of spring wheat and canola, and found better performance in canola than in spring wheat [18]. However, although the studies mentioned above have extracted several polarimetric parameters for crop growth monitoring and growth parameter inversion, their focus has been on retrieval of the later phenology. Therefore, the potential performance of polarimetric parameters in crops, particularly in rape, has not been fully explored.

Model algorithms also play a critical role in crop growth parameter inversion. Many algorithms have been developed, and all can be grouped into two broad categories of parametric or nonparametric algorithms. Parametric algorithms assume that the relationships between dependent (i.e., crop growth parameters) and independent (i.e., quad-polarimetric parameters) variables have explicit model structures. Examples include empirical regression models and canopy scattering models, such as the Water-Cloud Model (WCM). Nonparametric algorithms, which are also called machine-learning algorithms, replace model structure in a data-driven manner. These models include the random forest algorithm, artificial neural networks, and support vector regressions [25,26]. Among these

modelling algorithms, empirical regression models, which simplify the process of interaction between the vegetation canopy and microwaves, can retrieve the estimated parameters effectively and timeously; therefore, these linear or nonlinear algorithms have been applied in many previous studies [27–29]. In practice, the relationships between biomass and quad-polarimetric parameters are often complex. Sometimes several empirical regression models are suitable for parameter inversion [28]. To the best of our knowledge, no previous study has identified the most suitable empirical regression models through a detailed comparison of these algorithms. Meanwhile, previous estimation models were only built during the whole crop growth season or in special growth stages, and their interchangeability has also not been explored. The best performance of empirical regression models in rape biomass inversion and the interchangeability and suitability of these algorithms are still unknown.

Therefore, this study focused on the following: (i) sensitivity of quad polarimetric observables to rape biomass at each growth stage and during the entire growth cycle, using temporal Radarsat-2 data acquired during the whole growth season; (ii) the best estimation of rape biomass, with empirical regression models based on parameters selected from all of the extracted qaud-polarimetric variables; and (iii) the feasibility of using models built during the whole rape growth cycle instead of models built at each growth stage.

2. Materials

2.1. Test Site

The study site was located on farmland in Shangkuli (120.76°–120.89°E; 50.28°–50.39°N) in City Hailar, Inner Mongolia, which is in the northeast of China (Figure 1). The landscape is predominantly flat, with a slope of less than 1%. The whole study area is dominated by a Leached Chernoem soil with a sand clay silt texture (sand = 5.86%, clay = 42.8%, silt = 52.06%). The climate is classified as cold temperate continental monsoon, with a cold and dry long winter, whereas the short summer is warm and wet. Approximately 90% of the farmland supports one harvest per year. The principal crops cultivated in the study area are spring rape (*Brassica napus* L.) and wheat (*Triticum aestivum* and *Hordeum vulgare*). The specific species of rape cultivated at the test site was hybrid-5, which is quite common in the north of China. This crop is usually sown from May to June, reaching maturity in the middle of August, and is harvested in early September. The cultivation period lasts about 115–140 days.
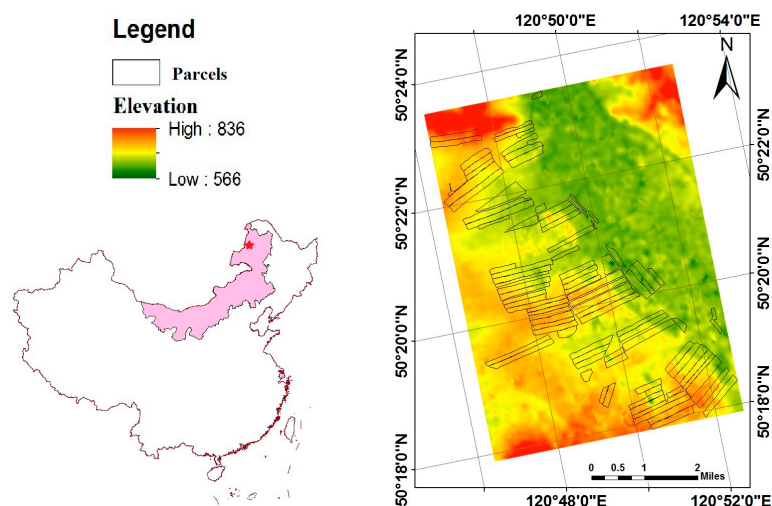
Figure 1. The test site in Inner Mongolia, China. The left subpanel shows the location of the Inner Mongolia Autonomous Region of China (in pink). The red star shows the location of the test site. The right subpanel shows the sample parcels in the test sites overlaid on the related topography (Digital Elevation Model).

2.2. Temporal Quad-Polarization Data and Ground Truth Data

In this study, five temporal Radarsat-2 quad-polarimetric single-looking complex (SLC) C-band (5.3 GHz) images were collected from 23 May 2013, to 27 August 2013, which covered the whole growth cycle of the rape crop. To build a time series in the most consistent way, all of the images were acquired with the same mode, beam, and orbit pass. Table 1 shows the detailed parameters of the SAR datasets.

Table 1. The details of five Radarsat-2 images.

Parameters	Values
Polarisation	Quad
Frequency	5.405 GHz
Incidence angle	37.4~38.8
Range pixel spacing	4.96 m
Azimuth pixel spacing	4.73 m
Orbit direction	Ascending
Beam mode	FQ18

Field data were collected concurrently with SAR acquisition. A set of 95 rape plots was used in this study. The size of the sample plots varied from 3.3 to 47.0 hectares; the average size was 18.6 hectares. The planting direction was west-east, and the row spacing was 30 cm. Information recorded during the field work included LAI, plant stem height, fresh and dry weight per m^2, plant water content, and global positioning system (GPS) location. The coordinate information of these samples was recorded with a Trimble Pathfinder DGPS, which was later co-registered with polarimetric SAR (PolSAR) data. The position precision was 50 cm. LAI ($m^2\,m^{-2}$) values were measured at three sample sites in each parcel with a LI-COR LAI-2200 instrument. To obtain LAI measurements, we took one measurement of the sky, and then four measurements of the lower part of the crop vegetation. Finally, one more measurement of the sky was taken. All of the LAI measurements were measured either in the early morning or late afternoon to reduce the effects of the sun. The three samples were chosen randomly. The volumetric water content ($m^3\,m^{-3}$) in the top 7.5 cm of the soil were also measured the same way as the LAI using a FieldScout time domain reflectometry soil moisture meter in high clay mode after its calibration. At each of the three sample sites, five soil moisture readings were taken and then 15 moisture readings were collected for each plot. Biomass samples were randomly collected in a square of 0.5 m × 2 rows in each plot. Then each biomass sample was weighed to determine the wet weight, and the value was recorded as wet biomass ($g\,m^{-2}$). Then it was dried at 95 °C for 48 h and weighed again. The new value was recorded as the dry biomass.

3. Methods

3.1. Quad-Polarization SAR Data Processing and Feature Extraction

A total of 27 quad-polarisation parameters were extracted from each of the SLC SAR datasets. They were grouped into three feature types: intensity-based parameters (HH, HV, and VV), Freeman–Durden decomposition-based parameters (ODD for surface scattering component, DBL for double-bounce scattering component, VOL for volume scattering component and ratio parameters derived from them), and Cloude–Pottier decomposition-based parameters such as each eigenvalue and other parameters derived from them (i.e., entropy and α). All of the features were multi-looked, filtered using PolSARPro software version 5.0, and orthorectified using MapReady. The data were multi-looked, with two in the azimuth direction and two in the range direction, and filtered using a 5 × 5 Boxcar filter to reduce speckle noise. The resulting pixel dimensions were about 9.92 × 9.46 m. A shuttle radar topographic mission 30 m (i.e., 1 arc second) digital elevation model (DEM) was used for SAR image simulation and registration, and for subsequent orthorectification of all of the features.

After orthorectification, all of the features were converted into the WGS-84 datum and UTM zone 50-north coordinate system. Figure 2 shows the SAR data processing procedure and study flowchart.
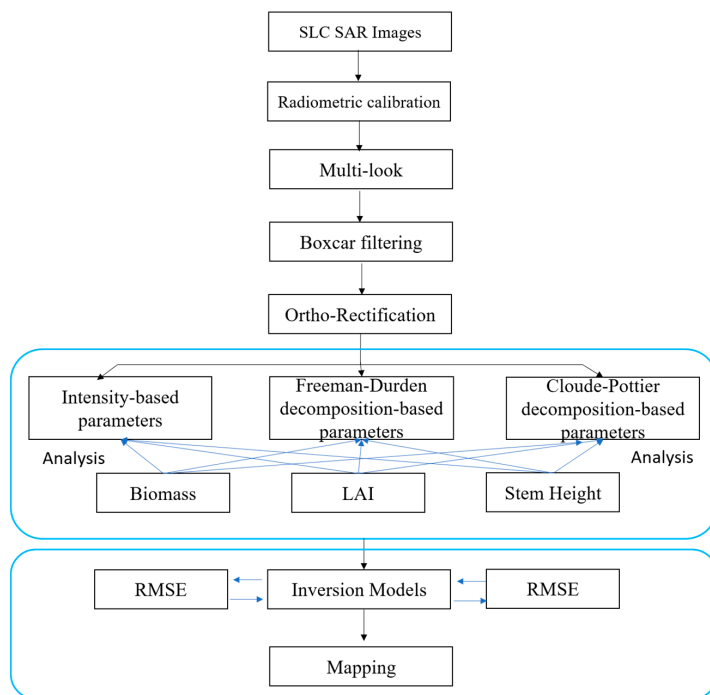
Figure 2. Synthetic aperture radar (SAR) data processing and the study flowchart. SLC, single-looking complex; LAI, leaf area index; RMSE, root mean square error.

3.1.1. Intensity-Based Parameters

The normalised radar cross-section (σ^0), which corresponds to the backscattering coefficient, was converted by the imaginary part (I) and real part (Q) of the signal for each polarisation (HH, HV, VH, and VV) in the tiff image file from each SLC data through Equation (1). Equation (2) interpreted the details of the radiometric calibration and how to keep the phase for further PolSAR data analysis.

$$\sigma^0 = \langle \frac{I^2 + Q^2}{A^2} \rangle \tag{1}$$

$$S2 = \begin{bmatrix} S_{HH} & S_{HV} \\ S_{VH} & S_{VV} \end{bmatrix}$$

$$= \begin{bmatrix} \frac{I_{HH}}{A} + i\frac{Q_{HH}}{A} & 0.5\left[\left(\frac{I_{HV}}{A} + i\frac{Q_{HV}}{A}\right) + \left(\frac{I_{VH}}{A} + i\frac{Q_{VH}}{A}\right)\right] \\ 0.5\left[\left(\frac{I_{HV}}{A} + i\frac{Q_{HV}}{A}\right) + \left(\frac{I_{VH}}{A} + i\frac{Q_{VH}}{A}\right)\right] & \frac{I_{VV}}{A} + i\frac{Q_{VV}}{A} \end{bmatrix} \tag{2}$$

$$S2 = \begin{bmatrix} S_{HH} & S_{HV} \\ S_{VH} & S_{VV} \end{bmatrix} \Rightarrow [T] = k_p k_p^{*T} = \frac{1}{2} \begin{bmatrix} S_{HH} + S_{VV} \\ S_{HH} - S_{VV} \\ S_{HV} + S_{VH} \\ i(S_{HV} - S_{VH}) \end{bmatrix} \times$$

$$\begin{bmatrix} (S_{HH} + S_{VV})^* & (S_{HH} - S_{VV})^* & (S_{HV} + S_{VH})^* & (S_{HV} + S_{VH})^* \end{bmatrix}.$$

$$\langle [T] \rangle = \lambda_1 e_1 e_1^* + \lambda_2 e_2 e_2^* + \lambda_3 e_3 e_3^*$$

where A is the gain, which only changes in the range direction and is provided as a look-up table in XML file format in each SLC data product file; S2 is the Sinclair matrix, and the subscripts correspond to all of the polarisation channels (e.g., HH, HV, VH, and VV). Because Radarsat-2

data are acquired in mono-static mode, we averaged S_{HV} and S_{VH} in Equation (2) to keep them equal [30]. As a result, in this study, only three backscattering coefficients ($\sigma^0_{HH}, \sigma^0_{HV}, \sigma^0_{VV}$) were calculated. The ratios between the three backscattering coefficients (i.e., $\sigma^0_{HH}/\sigma^0_{VV}$, $\sigma^0_{HV}/\sigma^0_{HH}$, and $\sigma^0_{HV}/\sigma^0_{VV}$), polarization difference ratio (i.e., PDR = $(\sigma^0_{HH} - \sigma^0_{VV})/(\sigma^0_{HH} + \sigma^0_{VV})$, and radar vegetation index (i.e., RVI = $8\sigma^0_{HV}/(\sigma^0_{HH,} + \sigma^0_{VV} + 2\sigma^0_{HV})$ based on backscattering coefficients were also extracted. The ratios of the backscattering coefficients were insensitive to surface roughness but were sensitive to the dielectric constant of the surface. PDR corresponding to scattering angle was also sensitive to materials with different dielectric constants [31]. The RVI describes the percentage scattering power from vegetation or soil [29,32].

3.1.2. Freeman–Durden Decomposition-Based Parameters

The Freeman–Durden decomposition is a technique for fitting a physically based, three-component scattering mechanism model to quad-polarimetric SAR observations without utilizing any ground truth measurements [33]. In this study, the symmetric covariance matrix (C3) calculated by the calibrated S2 was applied to extract three scattering mechanisms according to Freeman–Durden decomposition: vegetation scattering from randomly oriented dipoles (VOL), double-bounce scattering (DBL), and first-order Bragg surface scattering (ODD). The RVI based on three scattering mechanisms ($RVI_{Freeman}$ = VOL/(VOL + DBL + ODD)), and the ratios among VOL, DBL, ODD, and total scattering power (SPAN), as well as the ratio between VOL and ODD, were also extracted in this study. These ratios were reported to be sensitive to vegetation growth by Hao [25].

3.1.3. Cloude–Pottier Decomposition-Based Parameters

Cloude–Pottier decomposition [31] is based on eigenvalues and the eigenvector extraction of a coherency matrix (T), which is defined as an outer product of the corresponding scattering vectors in Pauli bases (Equation (3)). The key idea of this approach is the generalisation of the wave dichotomy to higher dimensional coherency matrices. According to symmetry theory, in this case we wrote the general depolarizing coherency matrix as the sum of three independent and orthogonal scattering mechanisms, as shown in Equation (4):

$$S2 = \begin{bmatrix} S_{HH} & S_{HV} \\ S_{VH} & S_{VV} \end{bmatrix} \Rightarrow [T] = k_p k_p^{*T} = \frac{1}{2} \begin{bmatrix} S_{HH} + S_{VV} \\ S_{HH} - S_{VV} \\ S_{HV} + S_{VH} \\ i(S_{HV} - S_{VH}) \end{bmatrix} \times$$

$$\begin{bmatrix} (S_{HH} + S_{VV})^* & (S_{HH} - S_{VV})^* & (S_{HV} + S_{VH})^* & (S_{HV} + S_{VH})^* \end{bmatrix} \tag{3}$$

$$\langle [T] \rangle = \lambda_1 e_1 e_1^* + \lambda_2 e_2 e_2^* + \lambda_3 e_3 e_3^* \tag{4}$$

where $\langle ... \rangle$ denotes averaging, λ_i is the real eigenvalue and has a direct physical interpretation in terms of the power scattering into the mechanism represented by e_i, e_i is the corresponding complex eigenvector and is parameterized by unitary transform. Two functions of these eigenvalues are widely used to measure wave depolarisation. The two functions are defined as Equation (5) and are named the scattering entropy (H) and anisotropy (A).

$$H = -\sum_{i=1}^{3} P_i \log_3 P_i \quad P_i = \frac{\lambda_i}{\sum_{i=1}^{3} \lambda_i} \quad 0 \le H \le 1$$

$$A = \frac{\lambda_2 - \lambda_3}{\lambda_2 + \lambda_3} \tag{5}$$

A zero value of entropy indicates a purely polarised wave. At the other extreme, an entropy value of one means that the maximum depolarisation occurs. A is a complementary parameter to H, and measures the relative importance of the second and third eigenvalues in this decomposition. A = 0

indicates two secondary mechanisms of approximately equal proportions, whereas A = 1 indicates that the second mechanism is greater than the third. Although H is sensitive to the polarised and depolarised component, it cannot be used to determine the different scattering mechanisms in the polarised component. Thus, α, which can also be extracted from eigenvector e_i, was selected as an indicator of the different scattering mechanisms in polarised components. H and α are also known as H/α decomposition. α ranges between 0 and 90 degrees, corresponding to a continuous change from surface scattering ($\alpha = 0°$), then to dipole or volume scattering ($\alpha = 45°$), and finally the double-bounce scattering ($\alpha = 90°$).

In this study, eigenvalues and their related probability ($\lambda_1, \lambda_2, \lambda_3$ and P_1, P_2, P_3), H, α, A, and RVI based on Cloude–Pottier decomposition (RVI_{Cloude}) were extracted as the polarisation variables RVI_{Cloude} is defined by Equation (6), and describes vegetation shape and direction according to the description of shape and direction in cylinder models.

$$RVI_{Cloude} = 4\lambda_3/(\lambda_1 + \lambda_2 + \lambda_3) \tag{6}$$

3.2. Ground Data Campaign

During the sowing campaign from 8 May 2013, to 31 May 2013, the local farmland administrator collected detailed measurements such as sowing dates, crop varieties, and whether the plots were ploughed before seeding or not. The days after sowing (DAS) of the 95 selected plots in this study were calculated according to the sowing dates and dates that SAR data were acquired. Daily precipitation was recorded by an automatic meteorological station (MidWest, WPH1-PH-6) placed in the centre of the farmland. The cumulative precipitation during the 7 days before each satellite acquisition are shown in Table 2 and Figure 3. Five concurrent ground measurement campaigns were conducted at each satellite overpass, with no lag of more than 1 day. In each ground measurement campaign, we recorded LAI, stem height, surface soil moisture, and biomass including fresh and dry weight per m^2 from 11 to 14 representative plots.

Table 2. Precipitation details.

| Date	Mean Value (mm)
2013/05/24	6.4
2013/06/16	45.3
2013/07/10	73.8
2013/08/03	180.2
2013/08/27	4.4
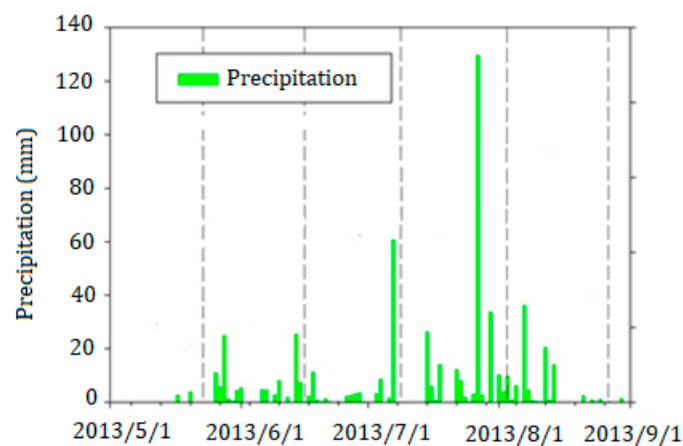
Figure 3. Daily precipitation (from 13 May 2014 to 30 August 2014). The five vertical dashed lines indicate synthetic aperture radar (SAR) observation dates (23 May, 16 June, 10 July, 3 August, and 27 August).

3.3. Temporal Polarimetric Response of Rape

The temporal polarimetric responses of rape biomass during the entire growth cycle were analysed as a function of the DAS. To overcome the intrinsic speckle effect, 27 polarimetric parameters for each plot were averaged at the plot level. Because these plots had different sowing dates (17 sowing dates as shown in Table 3), there were 85 different DAS for our five consecutive SAR acquisitions. To reduce the influence of uncontrolled factors on polarimetric parameters for the same DAS, mean values of all of the fields with the same DAS were calculated to analyse dynamic changes in the 27 polarimetric parameters. The shape and aspect of rape changed substantially during its growth cycle, which results in changes in its polarimetric scattering and biomass [2]. Thus, the entire growth cycle of rape was divided into five stages according to their Biologische Bundesanstalt Bundessortenamt und CHemische Industrie (BBCH) [25], SAR data acquisition date, and DAS. The details are showed in Table 3. Photographs of rape at each growth stage are shown in Figure 4.

Table 3. Principal stages of rape and the related Biologische Bundesanstalt Bundessortenamt und CHemische Industrie (BBCH) scales.

Acquisition Date	BBCH Stages	Principal Scales [DAS Range]	Soil Moisture (%)	Dry Biomass (g m^{-2})
2013/05/23	Germination (0)	P1 [−7, 15]	[19.2, 42.4] 32.7	-
2013/06/16	Leaf development (1) and formation of side shoots (2)	P2 [16, 39]	[32.5, 43.8] 37.8	[9.5, 89.0] 37.7
2013/07/10	Stem elongation (3), inflorescence emergence, (5) and flowering (6)	P3 [40, 63]	[34.1, 47.4] 41.7	[86.8, 350.9] 207.3
2013/08/03	Development of fruit (7)	P4 [64–87]	[41.0, 59.8] 56.3	[694.7, 2009.2] 1210.4
2013/08/27	Ripening (8) and senescence (9)	P5 [89, 110]	[22.4, 51.0] 41.3	[875.0, 2509.7] 1616.4
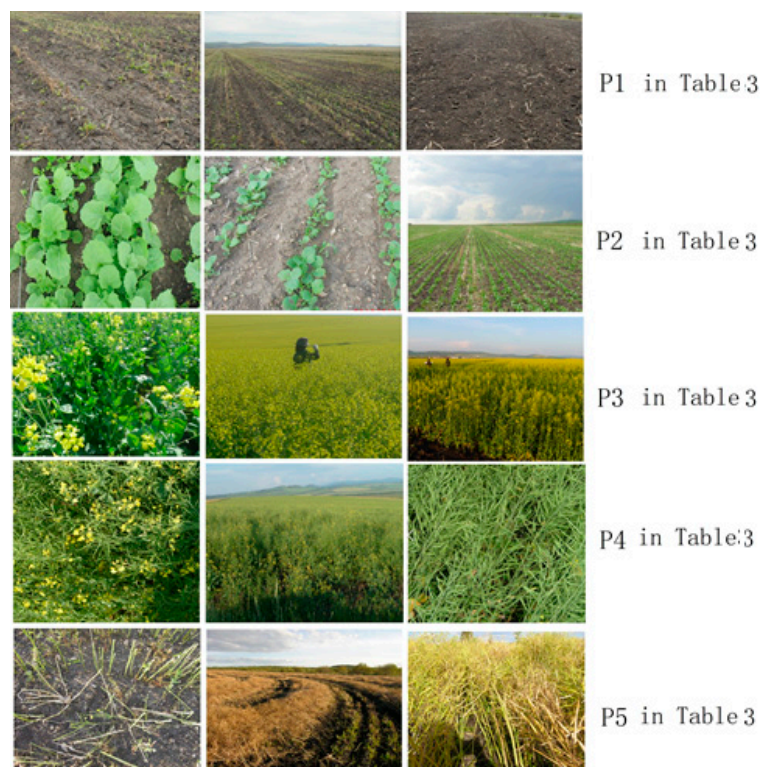
Figure 4. Typical oilseed rape fields at different growth stages. The text on the right of each line is their stage value.

3.4. Growth Parameters Inversion with Empirical Regression Models

The empirical regression models, which simplify the procedure of radiometric transfer and have great accuracy and feasibility in vegetation parameter inversion, were selected in this study for rape growth parameter inversion. Five traditional regression models were analysed in this study: linear (Equation (7)), quadratic (Equation (8)), power (Equation (9)), index (Equation (10)), and logarithm (Equation (11)). Statistical computations were conducted using the Statistical Product and Service Solutions software. The five models were run at different growth stages and for the entire growth cycle. All of the models were assessed within a significance level (P) of less than 0.05. The coefficient of determination (R^2) and RMSE (Equation (12)) were used to determine model effectiveness and validate the accuracy of the results. There were 44 samples used for determining biomass inversion and 33 samples used for determining LAI and stem height inversion during the whole growth cycle. Previous studies have inversed the growth parameters at different phenological stages due to the obvious different characteristics at the different growth stages. In this study, one of the objectives was to determine whether models that developed during the entire growth cycle could be substituted for models developed at each growth stage of the crop. Therefore, the main growth stages (i.e., P2, P3, and P4) of rape were chosen to analyse the substitutability of the models developed in the study. For each stage, 11 samples were used for the inversion of three growth parameters. Considering the small group of samples used for growth parameter inversion at each stage, only biomass was considered representative in this study. For the inversion procedure, two-thirds of the samples were used for building models, whereas one-third of the samples were used for the validation of results.

$$y = ax + b \tag{7}$$

$$y = ax^2 + bx + c \tag{8}$$

$$y = ax^b \tag{9}$$

$$y = ae^x \tag{10}$$

$$lny = alnx + b \tag{11}$$

where *a*, *b*, and *c* are the different index coefficients for each model, respectively, whereas *x* is the independent value and *y* is the dependent value. In this study, *x* included biomass, LAI, or stem height, and *y* included the 27 polarimetric parameters.

$$\text{RMSE} = \sqrt{\frac{1}{n-1} \sum_{i=1}^{n} (y_i - \hat{y}_i)^2} \tag{12}$$

where y_i and $\hat{y}_i$ are the measured and predicted values, respectively, and *n* is the number of samples.

4. Results

4.1. Sensitivity Analysis of Quad-Polarimetric Observables to Rape Growth Parameters

As described in the Methods section, a total of 44 samples were analysed in terms of the average DAS for each of the polarimetric observables during the entire rape growth cycle. They were plotted to describe the evolution of each polarimetric parameter, which was represented as a function of the DAS; the details are shown in Figure 5. Because one objective of this study was to identify the effective polarimetric parameters for monitoring rape growth, the results shown in Figure 5 also include plots of the evolution of biomass, LAI, and stem height. Figure 5 provides a description of their evolution for subplots a, b, and c. Considering the similar performance and physical meaning of some quad-polarimetric parameters, several representative polarimetric parameters are shown in Figure 5.
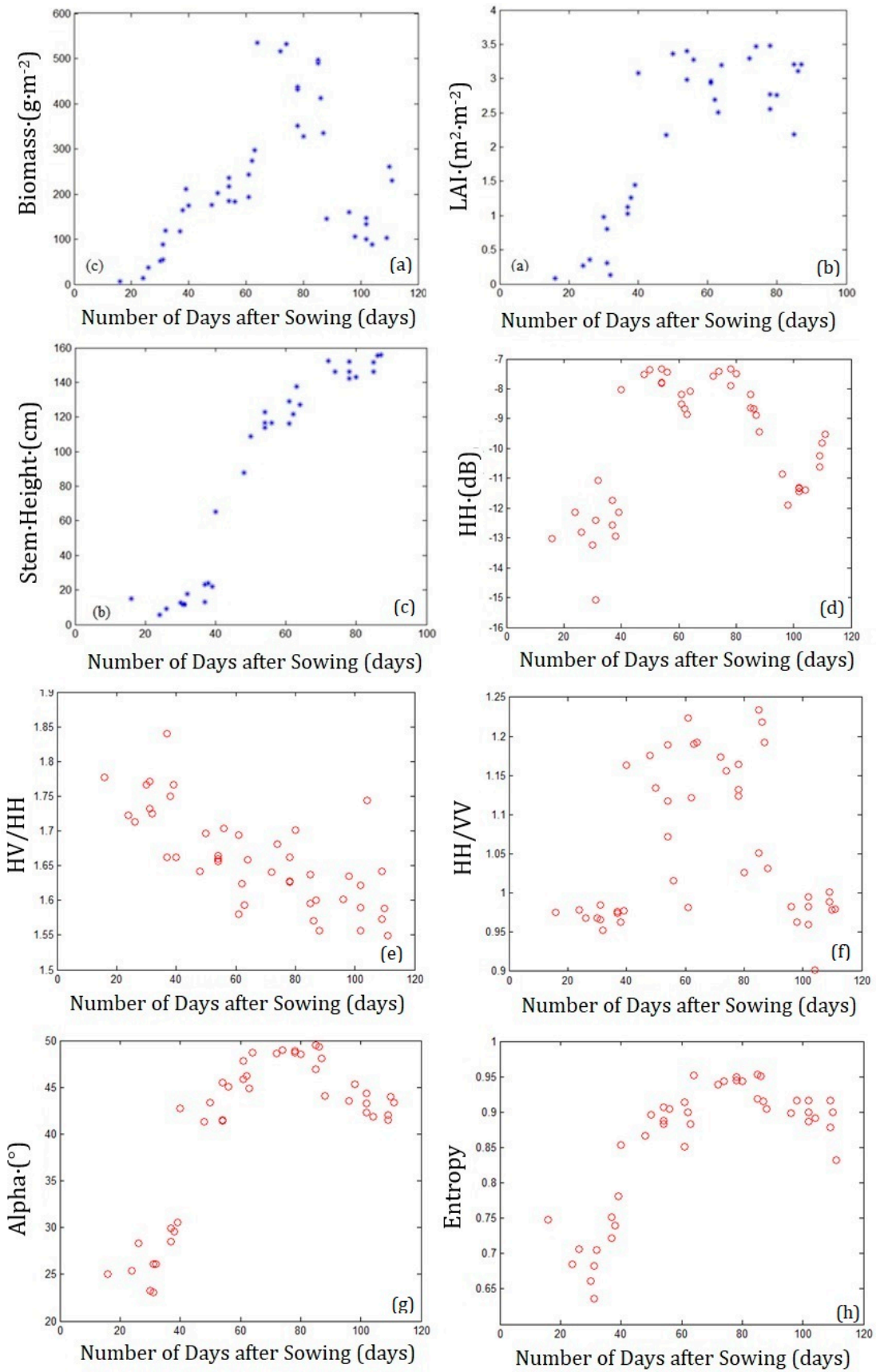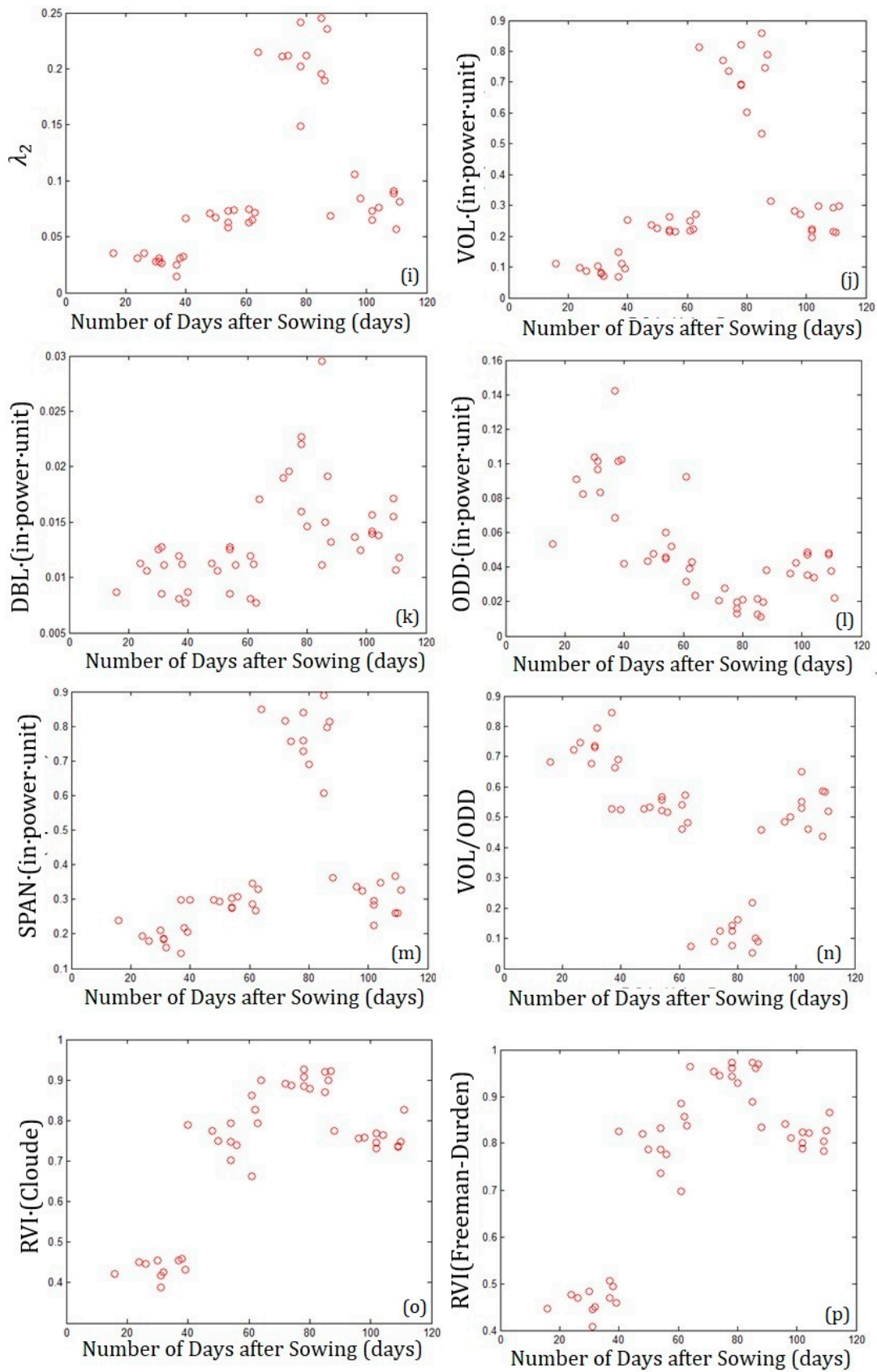
Figure 5. *Cont.*

Figure 5. Temporal evolution of three growth parameters and 27 quad-polarimetric parameters based on 95 plots during the entire growth cycle of rape. (**a**) Leaf area index (LAI); (**b**) stem height; (**c**) biomass. The following scatter plots are the representative quad-polarimetric parameters.

4.1.1. Analysis of the Sensitivity of the Quad-Polarimetric Parameters to Biomass

A detailed description of the evolution of the growth parameters was provided in our previous study [20]. From an analysis of the evolution of biomass and polarimetric parameters during the whole rape growth cycle (Figure 5a), several quad-polarimetric parameters were a good fit for biomass evolution trends. They included HH, VV, HV,α, H, λ_1, λ_2, λ_3, Vol, Span, RVI (Cloude), and RVI (Freeman). Among them, λ_2 and VOL were perfectly coincident with the evolution of biomass. λ_2, which represents the projection of a dihedral scattering mechanism on the HH-VV Pauli component, is the second eigenvalue of the coherence matrix T. It was indicated that the volume derived from the Freeman–Durden decomposition and double-bounce scattering described by an eigenvalue fluctuated in a similar manner to the biomass for the entire growth cycle and at different growth stages. By contrast, some quad-polarimetric parameters (e.g., RVI and A) were only weakly correlated with biomass evolution. RVI, which is based on the assumption of a strong double bounce occurring, was not suitable for the interpretation of the biomass response and displayed quite different trends.

4.1.2. Analysis of the Sensitivity of Quad-Polarimetric Parameters to LAI

Figure 5b shows a scatterplot of LAI against DAS during the whole rape growth cycle. From a comparison of the trend between quad-polarimetric parameters and LAI, the trends of RVI (Freeman), RVI (Cloude), α, P2, P3, HH, HV, and VV were found to exhibit a positive agreement with the evolution of LAI. Moreover, RVI (Freeman), RVI (Cloude), and α presented five different principal ranges during the entire cycle, and had trends perfectly coincident with the LAI, which were also confirmed by the correlation analysis results in Section 4.2. According to the definition of RVI (Freeman) and RVI (Cloude), they are the ratio of volume scattering power with total scattering power. The difference between them is the value of the volume scattering power. RVI (Freeman) was calculated by a Freeman–Durden decomposition, which was based on the physical scattering depolarisation models. RVI (Cloude) was derived from the eigenvalue decomposition, which was based on mathematics. The strong agreement of RVI (Freeman) and RVI (Cloude) with the evolution of LAI revealed a large sensitivity of the ratio between volume scattering power and total scattering power to the rape LAI. Because α represents a smooth scattering mechanism when a target is changed, the strong agreement between it and LAI indicated the sensitivity of LAI to target scattering mechanisms.

4.1.3. Analysis of the Sensitivity of Quad-Polarimetric Parameters to Stem Height

Figure 5c describes the evolution of stem height during the entire rape growth cycle. Stem height continued to increase before 75 DAS, and then the increasing tendency of the scatter plots tapered to a flat line until 95 DAS. From the monotone changes in the evolution of stem height it was clear that more quad-polarimetric parameters had a strong agreement with stem height than with biomass and LAI. Among all of the quad-polarimetric parameters, α, H, RVI (Freeman), and RVI (Cloude), which had similar trends from the beginning of the growth cycle to 75 DAS, displayed the strongest agreement with the evolution of stem height. The results also revealed that the quad-polarimetric parameters had a higher sensitivity to stem height than biomass and LAI. The likely reason for this might be the uncertainty or error transmission in the calculation of biomass and LAI, while there was no such influence on stem height, which was measured directly.

4.2. Empirical Regression Models Derived for Rape Growth Parameters

From the analysis in Section 3, the evolution of several quad-polarimetric parameters was in an obvious agreement with the evolution of rape biomass, LAI, and stem height, which indicated the potential for the use of empirical regression models for the inversion of those growth parameters. In this section, five traditional empirical regression models (linear, logarithmic, quadratic, power, and index models) were applied for the inversion of rape biomass, LAI, and stem height. The coefficients of determination and an analysis of their physical meaning are reported in Section 4.1, and our

previous study was used to select the best performing quad-polarimetric observables for the growth parameter inversion. Of the models tested, quadratic models had higher R^2 values than the other empirical regression models. However, the R^2 values of quadratic models were overestimated when the physical interpretations were related to the relationship between quad-polarimetric parameters and crop scattering mechanisms. Most logarithm and linear models, which had lower R^2 values than quadratic models and higher R^2 values than other empirical regression models, tended to provide a better physical interpretation of rape scattering mechanisms than quadratic models.

4.2.1. Empirical Regression Models Derived for Biomass

To build inversion models for rape biomass, 27 quad-polarimetric parameters were applied in the five empirical regression models. Table 4 shows the representative parameters that had R^2 values higher than 0.4 among the five regression models. The logarithmic and power models for HH, HV, and VV were computed by their inverse values. In Table 4, there are empty values for PDR because of the negative value for the construction of the logarithmic and power models. Of the five models, quadratic models, with high R^2 values, had the best performance for biomass inversion. For 16 quad-polarimetric parameters, there was a strong agreement with biomass, with R^2 values greater than 0.7. There was a moderate agreement for three parameters, with R^2 values between 05 and 0.7. The polarisation decomposition parameters indicated a strong performance in growth parameter inversion in the quadratic models, particularly VOL, λ_1, and λ_2. There were 10 quad-polarimetric observables with an R^2 value greater than 0.7 in the linear models, with the best one (VOL) with an R^2 value equal to 0.827. The best parameter for logarithm models was λ_3 with an R^2 value equal to 0.859. The lower R^2 values of the power and index models suggested their limited potential for biomass inversion.

Table 4. Coefficients of determination (r^2) of five empirical regression models for biomass inversion.

Polarization Observable	Linear	Logarithmic	Quadratic	Power	Index
HH/VV	0.4878	0.4937	0.5138	0.4438	0.4369
λ_1	0.6857	0.7044	0.7141	0.5135	0.4463
SPAN	0.8034	0.8155	0.8198	0.5076	0.4639
VOL/ODD	0.8034	0.8155	0.8198	0.5076	0.4639
λ_2	0.7984	0.7987	0.8334	0.5364	0.4768
VOL	0.8279	0.8337	0.8543	0.5844	0.4995
VV	0.4443	0.4233	0.4581	0.4766	0.5003
λ_3	0.7838	0.859	0.8686	0.7165	0.5049
HV	0.4812	0.4212	0.4813	0.4525	0.5225
P1	0.6863	0.71	0.7589	0.573	0.5678
P3	0.6922	0.6532	0.747	0.5667	0.5782
HH	0.518	0.4666	0.535	0.5332	0.589
P2	0.6728	0.6303	0.8125	0.572	0.5946
PR	0.7104	0.657	0.8089	0.6124	0.6281
ODD/SPAN	0.7037	0.8209	0.8147	0.5821	0.6334
RVI(Cloude)	0.7159	0.6753	0.7974	0.6267	0.6344
RVI(Freeman)	0.7301	0.6872	0.8114	0.6349	0.6412
Entropy	0.7092	0.6867	0.8003	0.6435	0.6517
Alpha	0.6873	0.6558	0.765	0.6793	0.6739

Note: SPAN, total scattering power; VOL, volume scattering component; ODD, first-order Bragg surface scattering; RVI, radar vegetation index.

The five empirical models for biomass inversion were also built with 27 quad-polarimetric parameters at the P2, P3, and P4 stages in this study. The quadratic models also performed better than the other empirical models in the models constructed at the different growth stages. However, the R^2 values of the models built at each stage were lower than those in the models built for the entire growth cycle. There were six quad-polarimetric parameters with R^2 values higher than 0.7 in the quadratic models, and three in the linear and logarithm models for biomass inversion at the P1 stage.

VOL had the best agreement with biomass, with an R^2 value of 0.828 at the P2 stage in the quadratic model. The best parameters for both the linear and logarithm models were λ_1, with R^2 values of 0.754 and 0.7701, respectively. At the P3 stage, only λ_2 had an R^2 value greater than 0.7 in the quadratic, linear, logarithm, and power models. The values were 0.834, 0.711, 0.730, and 0.781, respectively. The higher R^2 value between λ_2 and biomass revealed that the dominant scattering at the P2 stage was double-bounce scattering. It was also found that the Cloude–Pottier decomposition performed better than the Freeman–Durden decomposition for describing the rape scattering mechanism at this stage. At the P3 stage, RVI, which usually had a lower R^2 value in the inversion models for the entire growth cycle, was the only quad-polarimetric parameter with an R^2 greater than 0.7 in all five of the empirical regression models. This indicated that RVI was sensitive to biomass at this stage. Moreover, HH/VV, which had no effect on surface roughness but was dependent on the dielectric constant of the surface, also had a higher R^2 than the other parameters except RVI. The strong correlation between HH/VV and biomass revealed that the water content in rape changed regularly at the P3 stage.

4.2.2. Empirical Regression Models Derived for LAI

1. Five empirical regression models were applied to invert the LAI in this study. During the entire growth cycle of rape, 27 quad-polarimetric parameters were assessed against LAI using these regression models. Table 5 shows the parameters that had R^2 values higher than 0.4 for the five regression models. As with the inversion of biomass, quadratic models also produced a higher R^2 value than the other models. There were 16 polarimetric parameters with R^2 values greater than 0.7 in the quadratic models. However, some backscatter coefficients (e.g., HH and HV) had a strong agreement with the evolution of LAI. The results revealed that the sensitivity of backscatter coefficients to LAI was not the same as for biomass. There were 15 quad-polarimetric parameters with R^2 values greater than 0.7 in the linear models, which was larger than the corresponding number for biomass. Among these linear models, the highest R^2 value (0.831) was acquired by H. The best parameter for logarithm model inversion was RVI (Freeman), with an R^2 value of 0.843. The lower R^2 values in the power and index models implied that they were not suitable for LAI inversion. However, the results could have been affected by moisture conditions.

Table 5. Coefficients of determination (r^2) of five empirical regression models for Leaf area index (LAI) inversion.

Polarization Observable	Linear	Logarithmic	Quadratic	Power	Index
HH/VV	0.576	0.5888	0.7004	0.4567	0.4462
SPAN	0.5908	0.58	0.5918	0.4579	0.4737
VV	0.7749	0.7845	0.7942	0.5195	0.5086
P1	0.7448	0.7475	0.7511	0.519	0.5127
P2	0.7609	0.7521	0.7611	0.4972	0.5173
λ_2	0.7396	0.6779	0.7415	0.4505	0.5247
HH	0.7916	0.819	0.8551	0.5529	0.5299
VOL/ODD	0.6253	0.6273	0.6336	0.5441	0.5385
HV	0.7992	0.8188	0.8529	0.5584	0.5388
P3	0.7916	0.7826	0.7917	0.5259	0.5409
PR	0.8008	0.8116	0.8249	0.603	0.5968
Entropy	0.8313	0.8153	0.8684	0.5861	0.5996
VOL	0.8141	0.797	0.8156	0.6163	0.6228
ODD/SPAN	0.8216	0.7293	0.8547	0.5572	0.6322
RVI (Cloude)	0.8189	0.8394	0.8706	0.659	0.6361
RVI (Freeman)	0.8253	0.8431	0.8705	0.6698	0.6471
Alpha	0.8254	0.8274	0.8335	0.6765	0.6693

4.2.3. Empirical Regression Models Derived for Stem Height

Inversion models for stem height were built for biomass and LAI. Compared to biomass and LAI, more quad-polarimetric parameters had a strong sensitivity to stem height. Table 6 shows the parameters that had R^2 values higher than 0.6 for the five regression models. There were 17 polarimetric parameters for which there was a strong correlation with stem height, with R^2 values greater than 0.7. The R^2 values for α and H were higher than 0.9. It was noted that eigenvalues were not included in the polarimetric parameters with higher R^2 values. However, the eigenvalues of λ_2 and λ_3 were strongly correlated with stem height in the linear and logarithm models, with R^2 values greater than 0.7. The results also confirmed that an overestimation existed in the quadratic regression models.

Table 6. Coefficients of determination (r^2) of five empirical regression models for stem height inversion.

Polarization Observable	Linear	Logarithmic	Quadratic	Power	Index
HH/VV	0.626	0.6363	0.7013	0.6231	0.6128
SPAN	0.6836	0.6597	0.6868	0.7061	0.7274
VOL/ODD	0.6897	0.702	0.7153	0.748	0.7384
P3	0.7934	0.8006	0.8104	0.8006	0.7985
VV	0.809	0.7952	0.8091	0.7972	0.8074
P1	0.7767	0.7735	0.7768	0.8041	0.8078
λ_2	0.854	0.7817	0.8607	0.7281	0.8164
HH	0.8093	0.8159	0.8241	0.8312	0.8218
λ_3	0.7045	0.6769	0.7045	0.8099	0.822
HV	0.8477	0.8501	0.8543	0.8513	0.8458
P2	0.872	0.8717	0.8742	0.8467	0.8477
PR	0.8747	0.8806	0.8855	0.8598	0.8533
RVI(Cloude)	0.8783	0.8878	0.895	0.8756	0.863
ODD/SPAN	0.8784	0.8137	0.8897	0.7912	0.8673
RVI(Freeman)	0.88	0.8871	0.8929	0.8834	0.873
VOL	0.8656	0.8414	0.8658	0.8628	0.8774
Entropy	0.8881	0.8698	0.937	0.9104	0.9204

4.3. Mapping Results for Rape Growth Parameters

We analysed the R^2 values of all of the empirical regression models for each rape growth parameter in Section 4.2; the quadratic models with the three highest R^2 values and the linear or logarithm models with the highest R^2 values were selected to calculate their RMSEs. Table 7 shows the best models for each growth parameter inversion. The models with the lowest RMSE were selected as the most appropriate models for biomass, LAI, and stem height inversion. The inverted results at the P2, P3, and P4 stages were mapped in ArcGIS, and the related errors were also calculated and mapped. A similar procedure was applied to determine the most appropriate model for biomass inversion at each stage (Table 8). The difference between these two biomass inversion results was also analysed, with the results presented in Section 4.3.1.

Table 7. The best models for growth parameter inversion during the whole rape growth cycle.

|	Parameter	Model	R^2	RMSE
Biomass	VOL	$y = -590.51x^2 + 1043.5x - 0.275$	0.8543	109.93
LAI	RVI(Cloude)	$y = -22.106x^2 + 33.756x - 9.7948$	0.8706	0.56
Stem Height	Alpha	$y = 0.1306x^2 - 3.7836x + 22.944$	0.937	11.09

Table 8. The best models for biomass inversion at the P2, P3, and P4 stages

Parameter		Model	R^2	RMSE
P2	λ_1	y = 176.89ln(x) + 405.62	0.7707	74.32
P3	λ_2	y = 306851x^2 − 44149x + 1769.3	0.834	87.59
P4	PDR	y = 2839x + 334.32	0.7823	162.14

4.3.1. Mapping Results for Biomass

Biomass maps were produced for the P2, P3, and P4 stages and for the entire growth stage model of y = −590.51x^2 + 1043.5x − 0.275, with the models for the different stages being y = 176.89ln(x) + 405.62 for P2, y = 306851x^2 − 44149x + 1769.3 for P3, and y = 2839x + 334.32 for P4. These maps are shown in Figure 6. A comparison of estimation errors between two models at each stage is shown in Table 9. The spatial distribution of biomass in the maps calculated by the entire growth stage model were consistent with the biomass growth in the field campaign, but this was not the case for the biomass map calculated by the regression model at the P2 stage. In this stage, one-third of all of the plots on the map had a biomass higher than 300 g m^{-2}, which is not the actual case. The results were confirmed by the higher error in Table 8 at the P2 stage. At this stage, the estimation errors greater than 100 g m^{-2} were 45.5% for the regression model in the different stages, but were 18.2% for entire growth cycle regression model. The physical reason for this result was that soil scattering was more important than crop scattering because of the low crop cover at the P2 stage. With the growth of rape at the P3 and P4 stages, the backscattering signal from crops became larger than that from soil, and then the results for the regression models at each stage had a higher accuracy than the results from the entire growth cycle regression model. At the P3 stage, the results had an error of less than 25 g m^{-2} in 72.7% of plots when ODD was used with the linear model, but the figure was 45.5% in the model developed for the whole growth cycle. At the P4 stage, 36.3% of the models for different stages had errors of less than 25 g m^{-2} compared to zero for the entire growth cycle logarithm model.
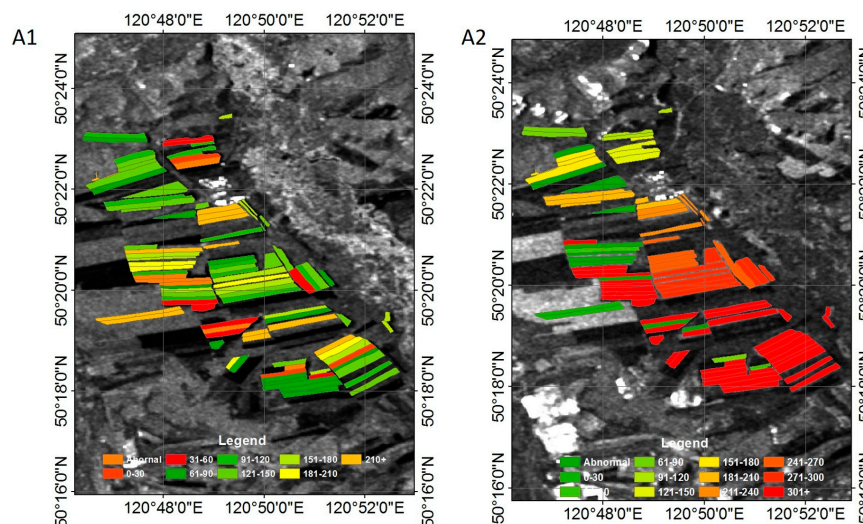
Figure 6. *Cont.*
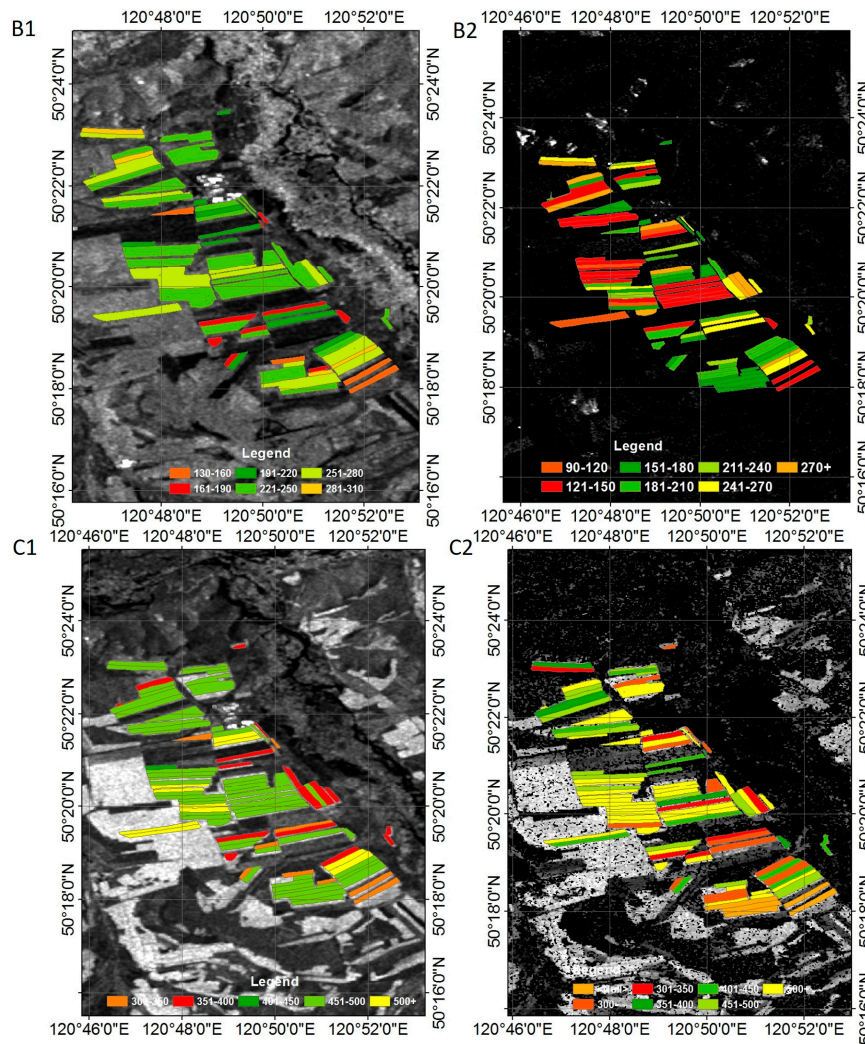
Figure 6. Biomass of 95 rape plots based on background images of quad-polarisation parameters used in their estimation models. (**A1**, **B1**, and **C1**) are the estimation results with models of $y = -590.51x^2 + 1043.5x - 0.275$ at the P2, P3, and P4 stages, respectively. The background images are the VOL parameter. (**A2**, **B2**, and **C2**) are the estimation results of the regression models at each stage. The background images for A2 are lambda $\lambda 1$, for B2 it is ODD, and for C2 it is HH/VV. The unit is g m^{-2}.

Table 9. The proportion of plots within each estimation error range for biomass at each stage with entire growth cycle regression models and models built at the P2, P3, and P4 stages.

Error Range (g m^{-2})	Date					
	20130616 (P2)		20130710 (P3)		20130803 (P4)	
	Entire	**Each**	**Entire**	**Each**	**Entire**	**Each**
0–25	36.3%	0.18%	45.5%	72.7%	0	36.3%
25–50	36.3%	0.09%	27.3%	18.2%	36.3%	18.2%
50–100	9.1%	27.3%	0	9.1%	27.3%	18.2%
100+	18.2%	45.5%	27.3%	9.1%	36.3%	27.3%

4.3.2. Mapping Results for LAI

The LAI results at the P2, P3, and P4 stages with the quadratic model built during the whole growth cycle are mapped in Figure 7. The LAI values in these maps were consistent with reality, with

continued growth during the P2 and P3 stages, which then remained stable at the P4 stage. Some plots had higher LAI values at the P3 stage, with a decrease at the P4 stage. This phenomenon was confirmed by the rape growth characteristics during these two stages. During these stages, large leaves in the bottom canopy layer began to wither and fall, which resulted in smaller and fewer leaves per unit volume, subsequently causing a decrease in the LAI. For the quadratic model, the high percentage of results within an LAI of 0–20 in Table 10 revealed its effectiveness for LAI inversion at each rape growth stage, particularly at the P2 and P3 stages. Table 10 shows a good performance for LAI inversion, with more than half of all plots having estimation errors of less than 0.5, but it also revealed a lack of sensitivity of RVI (Cloude) to LAI at the P4 stage. In this stage, with the elongation of the rape stem, it is difficult for RVI (Cloude) to respond to the change in rape scattering mechanisms, which was also confirmed by the dynamic changes in α and DBL. To obtain better inversion results, further investigations are needed in the future.
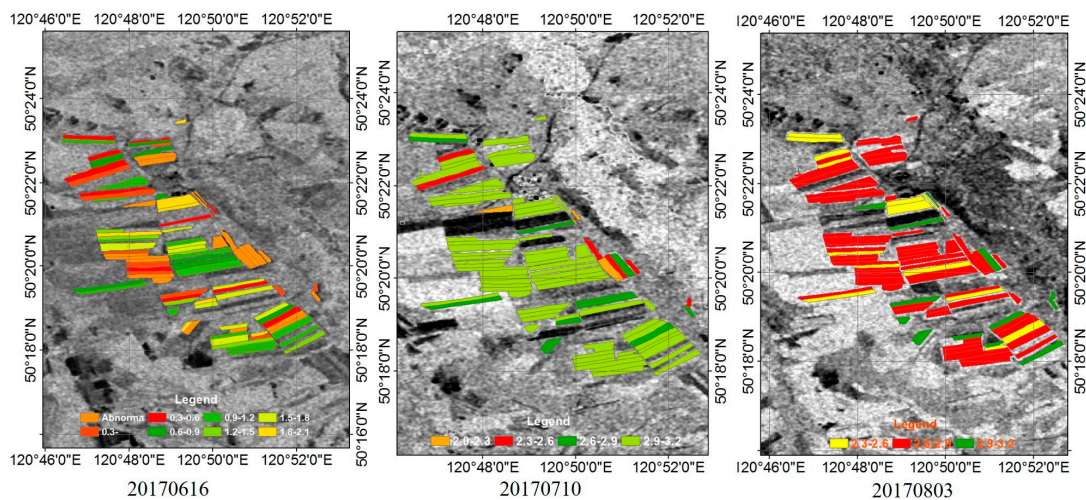
Figure 7. The leaf area index (LAI) of 95 rape plots, with a background image of the radar vegetation index (RVI) (Cloude). 20170616 is the estimation result of P2, 20170710 is the estimation result of P3, and 20170803 is the estimation result of P4. All of the results were estimated by y = $-22.106x^2$ + 33.756x $-$ 9.7948 with RVI (Cloude).
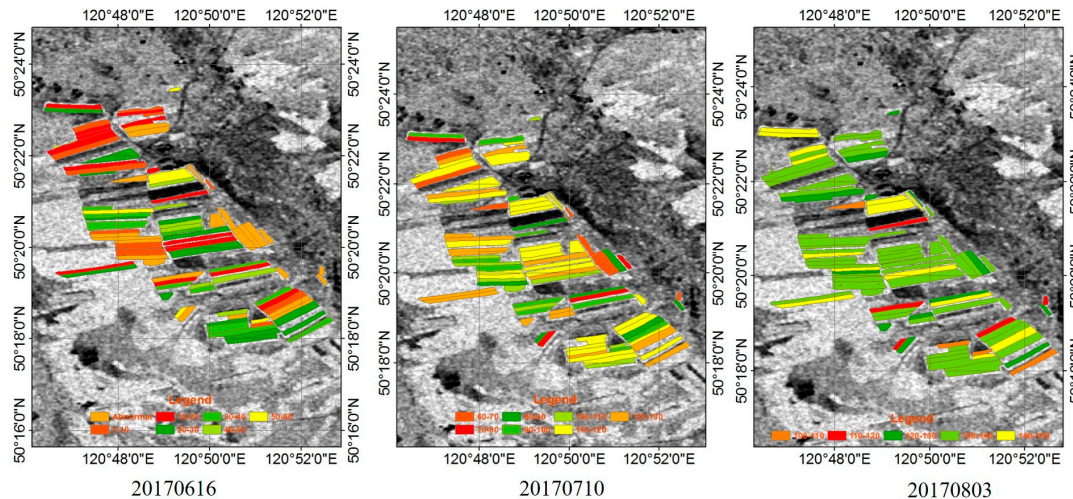
Table 10. The proportion of plots within each estimation error range for leaf area index (LAI) at each stage.

Error Range	Date		
	20130616	**20130710**	**20130803**
0–0.2	36.4%	36.4%	18.2%
0.2–0.5	18.2%	9.0%	45.5%
0.5–1	36.4%	45.5%	27.3%
1–1.5	9.0%	9.0%	9.0%

4.3.3. Mapping Results for Stem Height

The stem height results at the P2, P3, and P4 stages of each rape plot in the test site were mapped to demonstrate the potential of the selected regression model (Figure 8). The estimation errors (Table 11) also confirmed the effectiveness of this model. They also indicated that this model performed better at the P2 and P4 stages than at the P3 stages. In the P2 and P3 stages, there were 63.6% of plots with an estimation error less than 10 cm, whereas in the P4 stage, the figure was 45.5%. However, it should be noted that, at the P2 stage, despite the lower error ratio, the results showed an overestimation of stem height, which might have resulted from the dominance of soil scattering at this stage. The analysis

of the other polarimetric parameters indicated that the high estimation results in the P4 stage may have been caused by a change in the scattering mechanism following a change in the stem height. We therefore used different polarimetric parameters (e.g., VOL or SPAN) for stem height inversion to improve the estimation accuracy; however, further investigations are required in the future.

Figure 8. Stem height in 95 rape plots with the background image of scattering angle alpha (α). 20170616 is the estimation result of P2, 20170710 is the estimation result of P3, and 20170803 is the estimation result of P4. All of the results were estimated by $y = 0.1306x^2 - 3.7836x + 22.944$ with α.

Table 11. Proportion of plots within each estimation error range for stem height at each stage.

Error Range (g m^{-2})	Date		
	20130616	20130710	20130803
0–10	63.6%	63.6%	45.5%
10–20	9.0%	18.2%	27.3%
20–30	9.0%	9.0%	18.2%
30–40	18.2%	9.0%	9.0%

5. Discussion

To understand the sensitivity of polarisation information to rape biomass, LAI, and stem height, we extracted 27 polarisation parameters from SLC SAR datasets in the literature [1,2] and analysed their evolution as a function of DAS. From these analyses, we found that many C-band polarisation observables were significantly correlated with rape biomass, LAI, and stem height. Among them, HH, VV, HV, α, H, eigenvalues of T matrix, VOL, SPAN, RVI (Cloude), and RVI (Freeman-Durden) had strong agreement with the evolution of biomass. HH, VV, HV, α, P2, P3, RVI (Cloude), and RVI (Freeman) had high coincidence with the evolution of LAI. H, α, RVI (Cloude), and RVI (Freeman–Durden) displayed high sensitivity to stem height. These results also highlighted the different sensitivity of these parameters to rape biomass, LAI, and stem height. The good performance of several polarimetric parameters has also been reported for canola stem height and LAI inversion in the literature [1,2]. To determine the most effective empirical inversion models for the inversion of the three growth parameters, we compared the performance of the linear, logarithmic, quadratic, power, and exponential models through an analysis of their coefficients of determination and their physical relationship with scattering mechanisms. The results indicated that quadratic models performed better than the other models, with higher R^2 values. However, sometimes there was an overestimation. By contrast, linear and logarithmic models produced more stable estimation results. To determine the interchangeability of models built during the entire growth cycle with models built at each growth

stage, these five types of regression models were also built at the P2, P3, and P4 stages for biomass inversion. The models with the lowest estimation RMSE were selected for the inversion and mapping of rape biomass, LAI, and stem height. The results for the models built at each stage showed that when crop cover was high (e.g., the P3 and P4 stages) the models performed better than the models built during the entire growth cycle. However, this was not the case for the P2 stage, in which crop cover was low and soil scattering was dominant.

It is generally accepted that C-Band polarimetric data are useful for crop biomass and LAI retrieval [2–4,18,31,34,35]. LAI estimation errors (RMSE in $m^2 \; m^{-2}$) range from 0.63 to 0.97 [36]. Estimation errors for biomass range from 58.438 to 78.834 $g \; m^{-2}$ [37]. These results were confirmed in this study. However, because the scattering mechanisms of crops are determined by their structure, which vary by crop type, condition, and phenology, it is necessary to extract more polarimetric parameters to determine the most sensitive parameters for different crop types under different conditions and with different phenologies [2,11,18]. A report by the Department of Agriculture and Agri-Food of Canada demonstrated the sensitivity of many polarimetric parameters to the dry biomass of corn, canola, and soybean, but not spring wheat [2]. Their results also proved the different capability of polarimetric parameters for the growth parameter inversion of canola and spring wheat [18]. In their results, α produced the highest R^2 values with canola stem height, which was also the case in our study. Some studies have estimated crop height with a polarimetric interferometric technique and produced similar results to those in our study [6,12]. Rape is a broadleaf plant, with a very distinctive change in canopy structure throughout its growth cycle. Due to its differences to corn, rice, soybean, and wheat, most of the abovementioned studies are not completely comparable with our study. However, the polarimetric sensitivity analysis of rape growth parameters still yielded some similar results to those of other studies using C-Band data to determine the polarimetric response or phenology identity. In the current study, a logarithmic regression based on rape biomass achieved an R^2 value of 0.8337 for VOL. Wiseman also reported a significant correlation between biomass and VOL, with an R^2 value of 0.579 for canola [2]. VOL had the second highest R^2 value of all of the polarimetric parameters investigated in this study. The lower values of the correlation coefficient in this study were possibly caused by the different SAR data acquisition parameters, such as incidence angle, during the entire growth cycle [14,38]. The significant correlations between HH, VV, HV, α, and LAI and their fluctuation with crop types in this study were also confirmed by the results from other studies [10,14]. In previous studies, the R^2 values for different polarisation parameters fluctuated from 0.15 to 0.97. In the current study, most of values were in the 0.01–0.87 range. The sensitivity of polarisation parameters to stem height in the current study was in agreement with the results reported in other studies [32,38].

To the best of our knowledge, this study was the first to select suitable empirical regression models for crop growth parameter inversion with polarimetric observables by the comparison of five different empirical regression models. Wiseman et al. (2015) demonstrated the apparent differences in polarimetric parameters to wheat, soybean, canola, and corn, which revealed the necessity to choose suitable models for crop growth parameters inversion with polarimetric parameters [2]. The best model for biomass estimation during the whole growth cycle was a quadratic regression based on VOL, with an R^2 value of 0.854 and RMSE of 109.93 $g \; m^{-2}$. In comparison, Yanghao (2015) obtained best case biomass estimations, with an R^2 value of 0.79 and RMSE of about 91.7 $g \; m^{-2}$ in rape using a linear regression model [25]. Hosseini et al. (2015) also predicted crop biomass using the WCM on Radarsat-2, with a mean RMSE of 78.834 $g \; m^{-2}$; however, the crop investigated was wheat [37]. Several studies also used polarimetric parameters, and with other inversion models obtained a stem height inversion RMSE of 10.37 cm, LAI inversion RMSE of 0.48 and biomass inversion RMSE of 220 g/m^2 [20]. Although these studies obtained a better LAI and stem height estimation accuracy than the current study, more time was required to construct the algorithm model and calculation. Better results may be achieved with lidar, hyperspectral data, or unmanned aerial vehicle data [7,8]; however, data collection depends on weather conditions, which can prevent the continuous monitoring of crops. This study was also the first time the feasibility of using a model built during the whole

crop growth cycle was tested as an alternative to models built at each stage of crop growth. Most biomass estimation is performed at different crop growth stages, such as booting and anthesis [25,27]. The results of this study demonstrated the good performance of biomass inversion model built during the entire growth cycle. For this model, about 50% of the estimation errors were lower than 50 g m^{-2} at different rape growth stages, particularly in the early season at the P2 and P3 stages. The study also found a higher estimation accuracy for models built at each certain stage. The correlations between polarimetric parameters and crop biomass at different growth stages and the whole growth cycle in previous studies were also similar to the results of this study [2]. However, because there were few samples for parameter inversion at each growth stage the results may not be robust, and their reliability needs to be confirmed. The best model for LAI inversion in this study was the quadratic model, based on RVI (Cloude), with an R^2 value of 0.8705 and RMSE of 0.56. Jiao et al. (2011) obtained the best LAI estimation by linear regression based on pedestal height, with an R^2 value of 0.91 and RMSE of 0.22 [14]. The value was acquired with LAI samples between 0 and 3. Prevot et al. (1993) estimated LAI with a WCM using C-Band data, with an RMSE of 0.64. The best model for stem height estimation in this study was also a quadratic regression, but based on α, with an R^2 value of 0.937 and RMSE of 11.09 cm [34]. The results were similar to those of the stem height inversion of rice obtained with polarimetric interferometric SAR technology, reported by Esra et al. (2016), with an RMSE of 10–13 cm [6].

Maps of crop growth parameters at different growth stages provided the crop growth state. The error calculated from the maps clearly demonstrated the accuracy of the inversion models at different growth stages. Based on a comparison between estimated biomass maps and reference data, we found that rape biomass continued to increase during the P2 and P4 stages. Most of the estimation error was lower than 50 g m^{-2} revealing the inversion potential of the models built during the entire growth cycle and indicating the potential for the substitution of models built at each stage. These conclusions were also applicable to LAI and stem height inversions, although further analysis is needed.

Compared to studies conducted using soybean, rice, wheat, canola, and cotton, the results of this study were very promising given that growth parameter estimation obtained similar or even better accuracies in rape plots. According to the highest R^2 values between polarimetric observables and growth parameters acquired by different polarisation parameters for different crops, we demonstrated that polarisation sensitivity changes with crop type. From an analysis of the performance of five types of empirical regression models, it was found that the quadratic, linear, and logarithmic models had a better estimation ability and robust growth parameter inversion. Models built during the entire growth cycle had the potential to be substituted for models built at each growth stage, with moderate levels of accuracy (RMSE of 100 g m^{-2} for biomass).

6. Conclusions

We investigated the sensitivity of quad-polarimetric observables to rape growth parameters at each growth stage and during the entire growth cycle with temporal Radarsat-2 data acquired during the entire rape growth season. We also estimated growth parameters with suitable empirical regression models based on polarimetric parameters selected from all of the extracted quad-polarimetric parameters, and determined the feasibility of using models built during the entire growth cycle as an alternative to models built at each growth stage.

Significant correlations with high R^2 values between many polarimetric parameters and rape biomass, LAI, and stem height, demonstrated the sensitivity of polarimetric information to rape growth parameters. However, the dependence of polarimetric sensitivity on crop type and phenology stage was also obvious. The best empirical regression models were selected based on a comparison of R^2 values and the RMSE of linear, logarithmic, quadratic, power, and index models, and then were applied to estimate biomass, LAI, and stem height. The results showed that the quadratic regression model had the best performance for growth parameter inversion, while the linear and logarithm models were

also suitable for predicting rape growth parameters. However, some previous studies have shown that linear models had higher R^2 values than our results, which could be the result of precipitation conditions, which would cause an obvious change in SAR reflectance. This should be investigated in future studies. A comparison of the estimation results calculated by models built at each growth stage and the entire growth cycle demonstrated their interchangeability with moderate accuracy. Mapping the estimation results could also improve the interpretation of the replaceability of these two types of models.

The study identified a high sensitivity of polarimetric information to rape growth parameters and the strong potential for rape growth parameter inversion with empirical regression models. To make a contribution to global crop growth parameter inversion or yield prediction, the approach should be applied to other crop types, with consideration of their different structure, condition, and phenology. By analysing these differences, this approach could be extended and deployed in different crops. It should be noted that such an SAR analysis is only possible with quad-polarisation observations.

An obvious limitation of this study was the small number of samples used for biomass inversion at each growth stage. In future studies, more samples should be taken. The 24-day revisit time of Radarsat-2 includes several phenological intervals at each growth stage, and therefore some errors will be obtained in growth parameter inversion. Future studies should collect shorter revisit data, such as that from the RADARSAT Constellation Mission, which has a 12-day revisit time. This may improve the performance of growth parameter inversion at each stage and then increase the accuracy of future studies.

Author Contributions: Wangfei Zhang is the principal author of this manuscript; he wrote the majority of the manuscript and contributed during one phase of the investigation. The other co-authors contributed to the field logistics, the experimental work, the selection and interpretation of the methods, and some portions of the written manuscript. The order of the authors reflects their level of contribution.

Conflicts of Interest: The authors have no conflict of interest to declare.

References

1. Heuzé, V.; Tran, G.; Sauvant, D.; Lessire, M.; Lebas, F. *Rapeseed Meal*; Feedipedia: A Programme by INRA, CIRAD, AFZ and FAO; 2017; pp. 14–55.
2. Wiseman, G.; Mcnairn, H.; Homayouni, S.; Shang, J. RADARSAT-2 Polarimetric SAR Response to Crop Biomass for Agricultural Production Monitoring. *IEEE J. Sel. Top. Appl. Earth Obs. Remote Sens.* **2015**, *7*, 4461–4471. [CrossRef]
3. Knauer, K.; Knauer, K. Remote Sensing of Rice Crop Areas- A Review. *Int. J. Remote Sens.* **2013**, *34*, 2101–2139.
4. Dong, J.; Xiao, X. Evolution of Regional to Global Paddy Rice Mapping Methods: A review. *ISPRS J. Photogramm. Remote Sens.* **2016**, *119*, 214–227. [CrossRef]
5. Liu, J.; Pattey, E.; Miller, J.R.; Mcnairn, H.; Smith, A.; Hu, B. Estimating Crop Stresses, Aboveground Dry Biomass and Yield of Corn Using Multi-temporal Optical Data Combined with a Radiation Use Efficiency Model. *Remote Sens. Environ.* **2010**, *114*, 1167–1177. [CrossRef]
6. Erten, E.; Lopez-Sanchez, J.M.; Yuzugullu, O.; Hajnsek, I. Retrieval of Agricultural Crop Height from Space: A Comparison of SAR Techniques. *Remote Sens. Environ.* **2016**, *187*, 130–144. [CrossRef]
7. Wang, C.; Nie, S.; Xi, X.; Luo, S.; Sun, X. Estimating the Biomass of Maize with Hyperspectral and LiDAR Data. *Remote Sens.* **2016**, *9*, 11. [CrossRef]
8. Yao, X.; Wang, N.; Liu, Y.; Cheng, T.; Tian, Y.; Chen, Q.; Zhu, Y. Estimation of Wheat LAI at Middle to High Levels Using Unmanned Aerial Vehicle Narrowband Multispectral Imagery. *Remote Sens.* **2017**, *9*, 1304. [CrossRef]
9. Zalite, K.; Antropov, O.; Praks, J.; Voormansik, K.; Noorma, M. Monitoring of Agricultural Grasslands with Time Series of X-Band Repeat-Pass Interferometric SAR. *IEEE J. Sel. Top. Appl. Earth Obs. Remote Sens.* **2016**, *9*, 3687–3697. [CrossRef]

10. Cable, J.; Kovacs, J.; Jiao, X.; Shang, J. Agricultural Monitoring in Northeastern Ontario, Canada, Using Multi-Temporal Polarimetric RADARSAT-2 Data. *Remote Sens.* **2014**, *6*, 2343–2371. [CrossRef]

11. Dunne, S.C.; Mcnairn, H.; Monsivais-Huertero, A.; Judge, J.; Liu, P.W.; Papathanassiou, K. Radar Steele Remote Sensing of Agricultural Canopies: A Review. *IEEE J. Sel. Top. Appl. Earth Obs. Remote Sens.* **2017**, *10*, 2249–2273. [CrossRef]

12. Lopez-Sanchez, J.M.; Vicente-Guijalba, F.; Erten, E.; Campos-Taberner, M.; Garcia-Haro, F.J. Retrieval of Vegetation Height in Rice Fields Using Polarimetric SAR Interferometry with TanDEM-X Data. *Remote Sens. Environ.* **2017**, *192*, 30–44. [CrossRef]

13. Prasad, R. Estimation of Kidney Bean Crop Variables Using Ground-based Scatterometer data at 9.89 GHz. *Int. J. Remote Sens.* **2011**, *32*, 31–48. [CrossRef]

14. Jiao, X.; Mcnairn, H.; Shang, J.; Pattey, E.; Liu, J.; Champagne, C. The Sensitivity of RADARSAT-2 Polarimetric SAR Data to Corn and Soybean Leaf Area Index. *Can. J. Remote Sens.* **2011**, *37*, 69–81. [CrossRef]

15. Mcnairn, H.; Shang, J.; Jiao, X.; Deschamps, B. Establishing Crop Productivity Using RADARSAT-2. In Proceedings of the ISPRS International Archives of the Photogrammetry, Remote Sensing and Spatial Information Sciences, Melbourne, Australia, 25 August–1 September 2012; pp. 283–287.

16. Kim, Y.; Zyl, J.V. Vegetation Effects on Soil Moisture Estimation. In Proceedings of the 2004 IEEE International Geoscience and Remote Sensing Symposium, (IGARSS' 04), Anchorage, AK, USA, 20–24 September 2004.

17. Hosseini, M.; Mcnairn, H. Using Multi-polarization C- and L-band Synthetic Aperture Radar to Estimate Biomass and Soil Moisture of Wheat Fields. *Int. J. Appl. Earth Obs. Geoinf.* **2017**, *58*, 50–64. [CrossRef]

18. Canisius, F.; Shang, J.; Liu, J.; Huang, X.; Ma, B.; Jiao, X.; Geng, X.; Kovacs, J.M.; Walters, D. Tracking Crop Phenological Development Using Multi-temporal Polarimetric Radarsat-2 Data. *Remote Sens. Environ.* **2017**, in press. [CrossRef]

19. Mascolo, L.; Lopez-Sanchez, J.M.; Vicente-Guijalba, F.; Mazzarella, G.; Nunziata, F.; Migliaccio, M. Retrieval of Phenological Stages of Onion Fields during the First Year of Growth by Means of C-band Polarimetric SAR Measurements. *Int. J. Remote Sens.* **2015**, *36*, 3077–3096. [CrossRef]

20. Yang, Z.; Li, K.; Shao, Y.; Brisco, B.; Liu, L. Estimation of Paddy Rice Variables with a Modified Water Cloud Model and Improved Polarimetric Decomposition Using Multi-Temporal RADARSAT-2 Images. *Remote Sens.* **2016**, *8*, 878. [CrossRef]

21. Lopez-Sanchez, J.M.; Cloude, S.R.; Ballester-Berman, J.D. Rice Phenology Monitoring by Means of SAR Polarimetry at X-Band. *IEEE Trans. Geosci. Remote Sens.* **2012**, *50*, 2695–2709. [CrossRef]

22. Moran, M.S.; Alonso, L.; Moreno, J.F.; Mateo, M.P.C.; Cruz, D.F.D.L.; Montoro, A. A RADARSAT-2 Quad-Polarized Time Series for Monitoring Crop and Soil Conditions in Barrax, Spain. *IEEE Trans. Geosci. Remote Sens.* **2012**, *50*, 1057–1070. [CrossRef]

23. Liu, C.; Shang, J.; Vachon, P.W.; Mcnairn, H. Multiyear Crop Monitoring Using Polarimetric RADARSAT-2 Data. *IEEE Trans. Geosci. Remote Sens.* **2013**, *51*, 2227–2240. [CrossRef]

24. Lopez-Sanchez, J.M.; Vicente-Guijalba, F.; Ballester-Berman, J.D.; Cloude, S.R. Polarimetric Response of Rice Fields at C-Band: Analysis and Phenology Retrieval. *IEEE Trans. Geosci. Remote Sens.* **2014**, *52*, 2977–2993. [CrossRef]

25. Hao, Y. Study on Quantitative Crop Monitoring by Time Series of Fully Polarimetric and Compact Polarimetric SAR Imagery. Ph.D. Thesis, Chinese Academy of Forestry, Beijing, China, 2015.

26. Lu, D.; Chen, Q.; Wang, G.; Liu, L.; Li, G.; Moran, E. A Survey of Remote Sensing-based Aboveground Biomass Estimation Nethods in Forest Ecosystems. *Int. J. Digit. Earth* **2014**, *9*, 1–43.

27. Li'ai, W.; Zhou, X.; Zhu, A.; Dong, Z.; Guo, W. Estimation of Biomass in Wheat Using Random Forest Regression Algorithm and Remote Sensing Data. *Crop J.* **2016**, *4*, 212–219.

28. Jia, Y.; Li, B.; Cheng, Y.; Liu, T.; Guo, Y.; Wu, X.; Wang, L. Comparison between GF-1 images and Landsat-8 images in monitoring maize LAI. *Chin. Soc. Agric. Eng.* **2015**, *31*, 173–179.

29. Kim, Y.; Jackson, T.; Bindlish, R.; Lee, H.; Hong, S. Monitoring Soybean Growth Using L-, C-, and X-band Scatterometer Data. *Int. J. Remote Sens.* **2013**, *34*, 4069–4082. [CrossRef]

30. Zhang, W.; Li, Z.; Chen, E.; Zhang, Y.; Yang, H.; Zhao, L.; Ji, Y. Compact Polarimetric Response of Rape (*Brassica napus* L.) at C-Band: Analysis and Growth Parameters Inversion. *Remote Sens.* **2017**, *9*, 591. [CrossRef]

31. Cloude, S. *Polarisation Application in Remote Sensing*; Oxford University Press: Oxford, UK, 2010.

32. Van de Griend, A.A.; Wigneron, J.P. The b-factor as a Function of Frequency and Canopy Type at H-polarization. *IEEE Trans. Geosci. Remote Sens.* **2004**, *42*, 786–794. [CrossRef]

33. Freeman, A.; Durden, S.L. A three-component Scattering Model for Polarimetric SAR Data. *IEEE Trans. Geosci. Remote Sens.* **1998**, *36*, 963–973. [CrossRef]

34. Prévot, L.; Champion, I.; Guyot, G. Estimating Surface Soil Moisture and Leaf Area Index of a Wheat Canopy Using a Dual-frequency (C and X bands) Scatterometer. *Remote Sens. Environ.* **1993**, *46*, 331–339. [CrossRef]

35. Ferrazzoli, P.; Guerriero, L.; Schiavon, G. Experimental and Model Investigation on Radar Classification Capability. *IEEE Trans. Geosci. Remote Sens.* **1999**, *37*, 960–968. [CrossRef]

36. Bériaux, E.; Lambot, S.; Defourny, P. Estimating Surface-soil Moisture for Retrieving Maize Leaf-Srea Index from SAR Data. *Can. J. Remote Sens.* **2011**, *37*, 136–150. [CrossRef]

37. Hosseini, M.; Mcnairn, H.; Merzouki, A.; Pacheco, A. Estimation of Leaf Area Index (LAI) in Corn and Soybeans Using Multi-polarization C- and L-band Radar Data. *Remote Sens. Environ.* **2015**, *170*, 77–89. [CrossRef]

38. Inoue, Y.; Kurosu, T.; Maeno, H.; Uratsuka, S.; Kozu, T.; Dabrowska-Zielinska, K.; Qi, J. Season-Long Daily Measurements of Multifrequency (Ka, Ku, X, C, and L) and Full-polarization Backscatter Signatures over Paddy Rice Field and Their Relationship with Biological Variables. *Remote Sens. Environ.* **2002**, *81*, 194–204. [CrossRef]